

# Light4GS: Lightweight Compact 4D Gaussian Splatting Generation via Context Model

Mufan Liu<sup>1</sup> Qi Yang<sup>2</sup> He Huang<sup>1</sup> Wenjie Huang<sup>1</sup>  
 Zhenlong Yuan<sup>3</sup> Zhu Li<sup>2</sup> Yiling Xu<sup>1†</sup>  
<sup>1</sup>Shanghai Jiao Tong University <sup>2</sup>University of Missouri, Kansas City  
<sup>3</sup> University of Chinese Academy of Sciences

{sudo\_evan, huanghe0429, huangwenjie2023, yl.xu}@sjtu.edu.cn, {qiyang, lizhu}@umkc.edu  
 yuanzhenlong21b@ict.ac.cn

## Abstract

3D Gaussian Splatting (3DGS) has emerged as an efficient and high-fidelity paradigm for novel view synthesis. To adapt 3DGS for dynamic content, deformable 3DGS incorporates temporally deformable primitives with learnable latent embeddings to capture complex motions. Despite its impressive performance, the high-dimensional embeddings and vast number of primitives lead to substantial storage requirements. In this paper, we introduce a **Lightweight 4DGS** framework, called **Light4GS**, that employs significance pruning with a deep context model to provide a lightweight storage-efficient dynamic 3DGS representation. The proposed **Light4GS** is based on 4DGS that is a typical representation of deformable 3DGS. Specifically, our framework is built upon two core components: (1) a spatio-temporal significance pruning strategy that eliminates over 64% of the deformable primitives, followed by an entropy-constrained spherical harmonics compression applied to the remainder; and (2) a deep context model that integrates intra- and inter-prediction with hyperprior into a coarse-to-fine context structure to enable efficient multiscale latent embedding compression. Our approach achieves over 12× compression and increases rendering FPS up to 20% compared to the baseline 4DGS, and also superior to frame-wise state-of-the-art 3DGS compression methods, revealing the effectiveness of our **Light4GS** in terms of both intra- and inter-prediction methods without sacrificing rendering quality.

## 1. Introduction

Novel view synthesis (NVS) aims to reconstruct 3D scenes from only a collection of multi-view images and has become a hot spot in computer vision. Traditional

<sup>†</sup>Corresponding author: Yiling Xu.

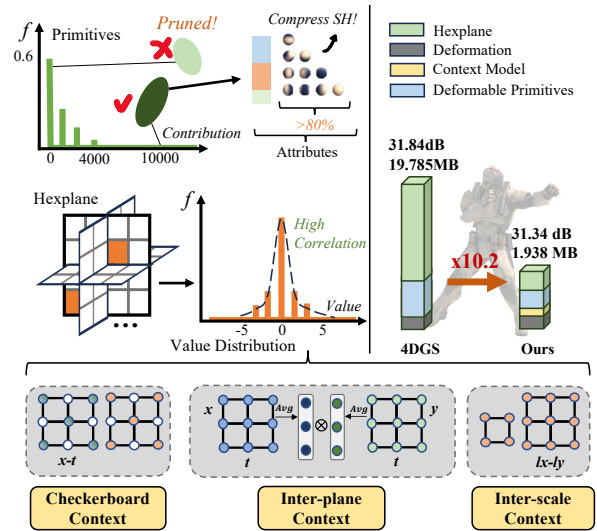


Figure 1. Motivation of 4DGS compression. Deformable primitives and hexplanes account for more than 99% of 4DGS’s storage (**top-right**). More than 60% of primitives show almost 0 contribution to the final rendering and the hexplane exhibits strong inter-correlation (**top-left**). Considering these, we introduce STP to prune insignificant primitives and employ MHCM to compress hexplanes, with the three key technical components (**bottom**).

NVS approaches often fail to provide a high-fidelity experience in real-time, as they suffer from complex structures [39] or cumbersome rendering processes [28]. Recently, 3D Gaussian Splatting (3DGS) [16] has gained great attention as a new NVS paradigm that achieves both state-of-the-art (SOTA) rendering quality and speed. By representing scenes with anisotropic Gaussian primitives, 3DGS enhances spatial expressiveness and adaptively refines photorealistic details across different viewports. Furthermore, its efficient differentiable splatting pipeline facilitates both rapid and explicit training, making 3DGS highly adaptable for interactive 3D applications.

With increasing demand for immersive experiences, extending 3DGS to dynamic scenes has become a growing research focus in this field. A straightforward approach involves training separate GS models for each timestamp, but this strategy quickly inflates storage, especially for long sequences. The time-variant 3DGS [21, 48] addresses per-frame training redundancy by modeling Gaussian attributes as time functions, albeit with significant training and storage costs. In contrast, the deformable 3DGS reduces modeling complexity by employing a small MLP to deform primitives trained from vanilla 3DGS. In this category, deformation of primitives is typically assisted by latent embeddings such as positional embeddings [2, 49], hash tables [45] and low-rank grids [43]. Among them, 4DGS [43] which utilizes multiscale hexplanes as latent embeddings is the most representative one. By mapping 4D space into six orthogonal planes, hexplane efficiently reduces computational complexity, making 4DGS more practical for real applications than the time-variant 3DGS. However, 4DGS’s storage requirements remain prohibitively high for real-world streaming. For instance, while current 5G networks stably support high-definition video at bitrates below 3 Mbps [23, 33], 4DGS requires 8–10 Mbps for comparable scenes. Fortunately, the two largest components of 4DGS show considerable redundancy and are prime candidates for compression. As illustrated in Fig. 1, over 60% of its primitives have minimal impact on rendering and can be pruned without loss in quality. Moreover, multiscale hexplanes exhibit strong correlations, suggesting that deep context modeling could greatly mitigate its information redundancy. Motivated by these insights, we aim to achieve effective 4DGS compression at a lightweight level.

In this paper, we propose **Light4GS**, a **lightweight 4D Gaussian Splatting** compression framework based on 4DGS [43], which leverages efficient pruning and deep context modeling. The motivation behind our approach is illustrated in Fig. 1. Our framework comprises two main modules: (1) a Spatio-Temporal significance Pruning method (STP) that reduces deformable primitives by evaluating their importance across different rendering views at all timestamps. STP not only saves storage but also streamlines training by automatically excluding gradients of both low-importance primitives and hexplane features. Since spherical harmonics (SH) coefficients account for over 80% of the primitive’s data volume, entropy-constrained compression is further applied to compress the SH; and (2) a Multiscale Hexplane Context Model (MHCM) that leverages intra- and inter-scale correlations to compress multiscale hexplanes: for the lowest-scale hexplane, a checkerboard context combined with either hyperprior or inter-plane context is employed to reduce spatio-temporal redundancies; high-scale hexplanes are compressed using inter-scale context in a coarse-to-fine fashion with reduced training complexity and

improved compression effectiveness. In summary, our contributions are three-fold:

- We propose the first lightweight 4DGS compression framework that integrates primitive pruning with a deep context model for storage-efficient dynamic 3DGS.
- We design a spatio-temporal significance pruning technique to prune redundant primitives and customized coarse-to-fine deep contexts to compress multiscale hexplanes. We also apply adaptive quantization during training and entropy constraints to compress SH.
- Experiments on synthetic and real-world scenes show Light4GS achieves 10-200x compression over SOTA dynamic NVS methods without sacrificing quality.

## 2. Related Works

**3DGS Compression:** Recent studies in 3DGS compression can be categorized into either post-processing-based or learning-based approaches. Post-processing methods include significance pruning [9, 18], codebooks [18], knowledge distillation [9], and quantization [30] to either prune primitives or compress Gaussian attributes. Thanks to 3DGS’s explicit structure, point cloud compression techniques such as octree encoding [15, 36], graph signal processing [47] and region-adaptive hierarchical transform (RAHT) [44] have also been adapted for 3DGS compression with structural considerations. Learning-based methods encompass strategies like Scaffold [26], which optimize neural Gaussians with residual components to reduce local redundancy, as well as entropy-constrained approaches [8, 24] that leverage global context for compressing 3DGS more effectively.

**Dynamic 3DGS:** While 3DGS has been successfully compressed, addressing the complexity of time modeling in dynamic 3DGS presents another challenge. Time-variant methods either decompose 4D Gaussians into time-conditioned 3D Gaussians with auxiliary components [48] or represent positions and attributes as functions of time to capture object motions [21]. Conversely, time-invariant (deformation-based) methods learn implicit position mappings that deform primitives using latent embeddings such as positional embeddings [2, 49], hash tables [45], and low-rank grids [43]. While the latter category achieves superior quality-storage performance, it lacks compact optimization for 3DGS as reviewed earlier and does not compress the latent embeddings, which we explore in the following.

**Latent Embedding Compression:** NVS methods utilizing latent embeddings [5, 11, 29, 38, 43] achieve high quality results, but also lead to increased storage overhead. To make embeddings smaller, [29] maps a large feature grid into a compact hash table, while [38] distills a high-dimensional feature grid into a binary grid. In dynamic NVS, storage overhead for latent embeddings become even more pronounced; low-rank approximations,

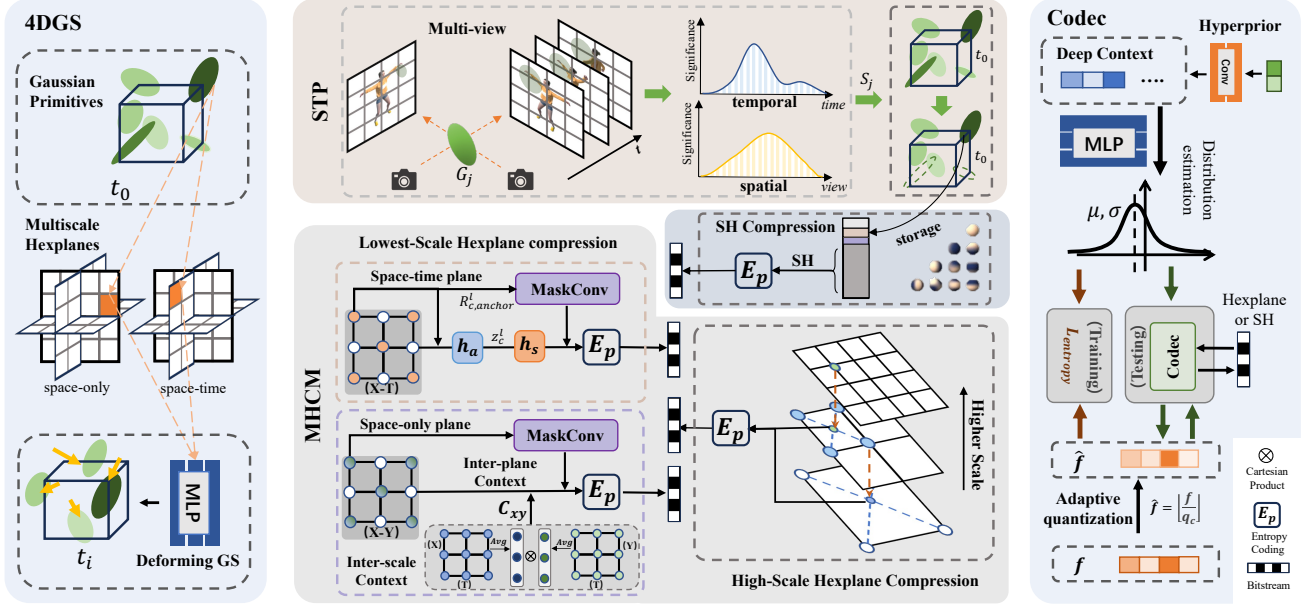


Figure 2. **Structure of Light4GS.** **Left:** Illustration of 4DGS. **Middle:** Storage reduction is achieved through STP and MHCM. Deformable primitives are pruned based on their spatio-temporal significance, while MHCM compresses multiscale hexplanes: the lowest-scale uses a checkerboard model with hyperprior or inter-plane context, and high-scales use inter-scale context. SH coefficients of remained primitives are further compressed via entropy-constrained coding. **Right:** Entropy-constrained codec pipeline, where deep context or hyperprior infers distribution prediction to encode/decode items  $f$  (multiscale hexplanes or SH). SH coding estimates distribution without any context.

such as wavelet decomposition [37], vector-matrix decomposition [6], and HexPlane projection [5, 11], provide promising solutions by mitigating dimensional redundancy. Moreover, contextual dependencies among neighboring elements provide further compression potential, as explored in image compression [13, 14], as well as in video compression [19]. To extend these advances into 3D representations, [7, 8] introduce spatial and hash-grid contexts to capture spatial redundancy in neural radiance field (NeRF) and 3DGS latent embeddings, which achieve nearly 100 compression gain over their vanilla implementations. Building on 3DGS and latent embeddings compression, our approach benchmarks 4DGS compression by training lightweight deformable primitives with a deep context model to fully exploit spatio-temporal redundancy.

### 3. Preliminary

**3DGS:** 3DGS represents a 3D scene using a collection of anisotropic Gaussian primitives distributed in space. Each primitive is characterized by a mean position  $\mu \in \mathbb{R}^3$  and a covariance matrix  $\Sigma \in \mathbb{R}^{3 \times 3}$ , defined as:

$$\mathbf{G}(\mathbf{x}) = e^{-\frac{1}{2}(\mathbf{x}-\mu)^\top \Sigma^{-1}(\mathbf{x}-\mu)}. \quad (1)$$

For differentiable rasterization, the covariance matrix  $\Sigma$  is decomposed into a rotation matrix  $\mathbf{R}$  and a scaling matrix  $\mathbf{S}$ . Each primitive is characterized by its color  $c_i \in \mathbb{R}^k$  (parameterized by  $k$  SH coefficients) and opacity  $\alpha \in [0, 1]$ .

During rendering, the primitives are splatted onto the viewing plane, and the final pixel color  $C$  is computed by blending the splatted primitives as:

$$C = \sum_{i=1}^N c_i \alpha_i \prod_{j=1}^{i-1} (1 - \alpha_j), \quad (2)$$

where  $N$  is the number of primitives contributing to that pixel.

**4DGS:** To handle dynamic scenes with temporal variations, deformable 3DGS, i.e. 4DGS, extends 3DGS by deforming its static primitives. The key idea is to compute the canonical-to-world mapping of each primitive over time by a deformation network  $\Phi$ :

$$\Delta \mathbf{G} = \Phi(f_h, t). \quad (3)$$

Here,  $f_h$  represents the hexplane feature of primitive  $\mathbf{G}$ . Each primitive deformed at  $t$  is computed by adding its deformation as:

$$\mathbf{G}' = \mathbf{G} + \Delta \mathbf{G}. \quad (4)$$

As mentioned earlier, learnable multiscale hexplanes are introduced in 4DGS to better capture dynamic variations and assist deformation prediction (see Fig.2). Specifically, it factorizes four dimensions in a deformation field into six planes at different scales:  $\mathbf{R}_c^l \in \mathbb{R}^{h \times l N_1 \times l N_2}$ ,  $c \in (\frac{x, y, z, t}{2})$ , where  $h$  is the hidden dimension of the feature,

$(N_1, N_2)$  is the basic resolution,  $l$  is the scaling factor and  $c$  is the pair-wise dimension combination. Each primitive’s coordinates  $\mu$  are combined with timestamp  $t$  to query each feature plane  $\mathbf{R}_c^l$ , where the four nearest features are retrieved and bilinearly interpolated. The interpolated features from all planes are element-wise multiplied, and concatenated from multiple scales to form the final hexplane feature  $f_h$ :

$$f_h = \bigcup_l \prod \text{interp}(\mathbf{R}_c^l(\mu, t)), \quad c \in \binom{x, y, z, t}{2}. \quad (5)$$

‘interp’ denotes the bilinear interpolation for querying the coordinate  $(\mu, t)$  located at 4 vertices of the feature plane.

## 4. Method

We present a storage-efficient deformable 3DGS compression framework that combines STP to reduce deformable primitives with MHCM for compressing multiscale hexplanes. For further optimization, the framework employs entropy-constraint SH compression and adaptive quantization to tailor the quantization of different plane types. We begin with an introduction to our pruning strategy, i.e., STP, in Sec. 4.1, followed by a detailed description of our deep context model and its coding process, i.e., MHCM, in Sec. 4.2. The remaining sections address our optimization techniques and loss functions.

### 4.1. STP: Spatio-temporal Significance Pruning

Vanilla 4DGS reduces computation and storage overhead by pruning low-opacity primitives during training. However, this approach overlooks each primitive’s *impact range* on view rendering; high-opacity primitives, for instance, might affect only a few pixels. Additionally, primitives that cover a large portion of pixels in one frame may contribute minimally in the next. Ignorance of these factors leads to limited effectiveness of the primitive pruning.

For this concern, a critical challenge in 4DGS is accurately capturing the global impact of each primitive on rendering quality. In 4DGS, each primitive is capable of deforming over time to account for scene dynamics, and this deformability enables us to assess the significance of one primitive across multiple frames. Building on this capability, we propose a spatio-temporal pruning strategy (STP) that evaluates each Gaussian’s contribution by calculating its intersection with viewing pixels over all timestamps. The global significance score of the  $j$ -th deformable primitive  $S_j$  is defined by aggregating its contributions across all timestamps and views as:

$$S_j = \sum_{t=1}^T \sum_{i=1}^{MHW} \mathbf{1}(\mathbf{G} + \Phi(f_h, t), r_{i,t}) \cdot \sigma_j \cdot \gamma(\Sigma_{j,t}), \quad (6)$$

where  $M$  is number of views at each timestamp,  $H, W$  are height and width of the rendered view.  $\mathbf{1}(\cdot)$  is an indicator function that returns 1 if the deformed primitive intersects with the viewing ray  $r_{i,t}$  at timestamp  $t$ , and 0 otherwise.  $\sigma_j$  is the opacity of the primitive, and  $\gamma(\Sigma_{j,t})$  is the normalized volume of primitive  $j$  calculated from its covariance matrix  $\Sigma_{j,t}$  at time  $t$ . During training, we periodically rank deformable primitives according to their spatio-temporal significance scores,  $S_j$ , and prune the least significant ones based on a predefined ratio. This approach greatly improves training efficiency by reducing the number of primitives to be processed, while optimizing the remaining primitives. Consequently, the retained primitives adapt to mitigate any potential quality loss from STP, preserving rendering quality despite the reduced model complexity.

### 4.2. MHCM: Multiscale Hexplane compression with Context Model

We use deep context model to reduce information uncertainty within multiscale hexplanes to achieve a minimized entropy loss. Specifically, each hexplane feature is modeled as a Gaussian distribution conditioned on a carefully designed deep context. This context-conditioned distribution is parameterized by a deep network (denoted as MLP() here for simplicity), which takes the context as input to predict each feature’s distribution parameters. These parameters are then used to compute the entropy of hexplane features, and subsequently encode features using Arithmetic Coding (AC) [17]. The total entropy is incorporated into the 4DGS optimization to balance the rate-distortion (RD) trade-off. In Light4GS, we propose a Multiscale Hexplane Context Model, MHCM that leverages intra- and inter-scale redundancies to compress multiscale hexplanes. Due to the mirroring nature of encoding and decoding, we present the context model from the encoding perspective, elaborating it in a coarse-to-fine manner in the following.

**Lowest-Scale Hexplane Compression:** Planes in one hexplane can be divided into two groups based on their dimensions: *space-only* and *space-time*. Throughout the lowest-scale encoding process, both groups employ checkerboard modeling but use different hyperpriors based on the availability of prior information. In this approach, we designate odd positions on each plane as anchors, which are encoded with only the hyperprior. In contrast, non-anchors (even positions) are encoded using both the hyperprior and the checkerboard context that is derived by applying masked convolution on the plane anchors. Without loss of generality, we omit the superscript  $l$  in this section, as it is always equal to 1. To compress the space-time group, since no prior information is available, we directly use a deep network  $h_a(\cdot)$  to extract hyperpriors as  $\mathbf{z}_c = h_a(\mathbf{R}_c)$ . The hyperprior is then applied to encode space-time planes as:

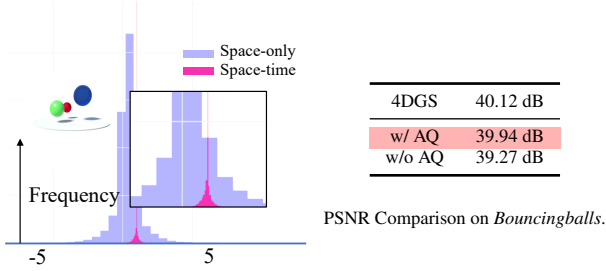


Figure 3. Distribution of space-time and space-only planes. Applying AQ achieves rendering quality improvement.

$$\Phi_c = \begin{cases} \text{MLP}(h_s(\mathbf{z}_c), \mathbf{0}), & \text{if } \mathbf{R}_c \in \text{anchors}, \\ \text{MLP}(h_s(\mathbf{z}_c), \text{MaskConv}(\mathbf{R}_c)), & \text{otherwise.} \end{cases} \quad (7)$$

$\Phi_c$  is the distribution parameters for  $\mathbf{R}_c$ ,  $h_s(\cdot)$  is the hyperprior decoding network and ‘MaskConv’ denotes applying convolution on the anchors. We prioritize encoding the space-time planes, as they capture both spatial and temporal information. Once decoded, their time-averaged values provide the *inter-plane context*, which serves as the hyperprior for the space-only planes. This eliminates the need for additional hyperprior storage and aids with decoded spatial information. To obtain the inter-plane context, consider an example where  $c = xy$  as shown in Fig. 2; each inter-plane context at  $(x, y)$  is obtained by first computing the time-average of features at  $(x, t)$  and  $(y, t)$ , then taking their Cartesian product. The inter-plane context  $\mathbf{C}_c$  is constructed to match the dimensionality of the decoded hyperprior,  $\text{MLP}(h_s(\mathbf{z}_c))$ , and thus replaces the decoded hyperprior in Eq. (7) for coding space-only planes.

**High-Scale Hexplane Compression:** High-scale hexplanes often exhibit significant redundancy with their lower-scale counterparts. Relying solely on the checkerboard model for compression overlooks these inter-scale redundancies, as it captures only intra-scale correlations. To address this issue, we introduce an *inter-scale context* that encodes higher-scale planes in a coarse-to-fine order. Specifically, higher-scale planes are decoded using context obtained from bilinear interpolation of its predecessor, as illustrated in Fig. 2. The distribution parameters for higher-scale features  $\mathbf{R}_c^{l+1}$  are predicted as:

$$\Phi_c^{l+1} = \text{MLP}(\text{interp}(\mathbf{R}_c^l, \mathbf{R}_c^{l+1}), \mathbf{0}). \quad (8)$$

Here, ‘interp’ denotes bilinear interpolation to query the coordinates  $\mathbf{R}_c^{l+1}$  located at the four vertices of  $\mathbf{R}_c^l$ . This progressive refinement greatly reduces redundancy and simplifies the deep context training.

### 4.3. Adaptive Quantization

In deep context modeling, each feature is quantized before being processed by the distribution estimation network.

However, conventional deep context modeling uses a fixed quantization step size of 1, which is unsuitable for multi-scale hexplanes due to their different value range. Additionally, space-only and space-time planes in 4DGS exhibit distinct means and variances owing to differences in spatial and temporal scales as shown in Fig. 3). To address this, we propose an Adaptive Quantization (AQ) method in which different learnable quantization steps  $q_c$  are assigned to the two groups during 4DGS training. According to [3], quantization can be approximated as adding uniform noise over the quantization range to enable differentiable training. This is illustrated in the total entropy loss for multiscale hexplanes as:

$$R_{\text{Hex}} = -\log_2 \left( \prod_l \prod_c \mathcal{N}(\Phi_c^l) * \mathcal{U}\left(-\frac{1}{2}, \frac{1}{2}\right)q_c \right), \quad (9)$$

where  $\mathcal{N}$  calculates the total probability distribution of the feature plane  $\mathbf{R}_c^l$  based on its predicted parameters,  $q_c$  is the learnable quantization step for plane  $c$ , and  $\mathcal{U}$  denotes the uniform distribution with unit range.

### 4.4. Entropy-constrained Compression for SH

Given that SH coefficients account for over 80% of each primitive’s storage, we utilize a fully factorized entropy model [3] to compress them directly. Specifically, each SH coefficient  $c_i$  of a primitive has its probability predicted by the *entropy bottleneck* and is then encoded using AC. The cumulative entropy loss of the SH coefficients  $R_{\text{SH}}$  is combined with the hexplane entropy loss  $R_{\text{Hex}}$  to form the total entropy loss  $L_{\text{entropy}}$ .

**Training Loss:** The overall training loss comprises three terms: the image reconstruction loss  $L_{\text{PSNR}}$ ; the total entropy loss  $L_{\text{entropy}}$  and the spatio-temporal regularization term  $L_{\text{ST}}$  from [5], which encourages smooth transitions in the deformation field. The total loss is given by:

$$L = L_{\text{PSNR}} + \lambda L_{\text{entropy}} + \alpha L_{\text{ST}}, \quad (10)$$

where  $\lambda$  and  $\alpha$  control the trade-off between compression efficiency and temporal smoothness.

## 5. Experiment

In this section, we describe the implementation details, perform comparisons with previous methods on three benchmark datasets, and evaluate the rate-distortion performance of Light4GS along with a comprehensive ablation study.

### 5.1. Experimental Configuration

Our model is based on the 4DGS framework [43] using PyTorch [34] and is trained on a single NVIDIA RTX 3090 GPU. We have fine-tuned our initialization and optimization parameters based on the configuration outlined in [43].

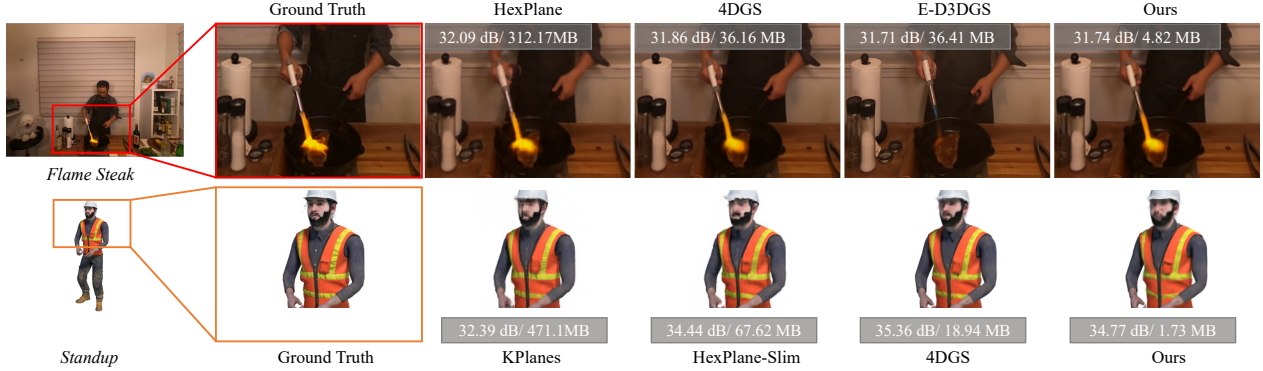


Figure 4. Qualitative quality comparisons of *Standup* in the D-NeRF dataset and *Flame Steak* in the Neu3D dataset. Light4GS achieves up to **65-272** $\times$  compression with a maximum 1% PSNR degradation. E-D3GS is excluded from the D-NeRF comparison as it is designed only for multi-camera setups.

Table 1. Quantitative results on D-NeRF dataset. The best and the second best results are denoted by red and blue.

| Model             | PSNR(dB) $\uparrow$ | SSIM $\uparrow$ | LPIPS $\downarrow$ | Training time $\downarrow$ | FPS $\uparrow$ | Storage (MB) $\downarrow$ |
|-------------------|---------------------|-----------------|--------------------|----------------------------|----------------|---------------------------|
| TiNeuVox-B [10]   | 32.67               | 0.97            | 0.04               | 28 mins                    | 1.5            | 48                        |
| KPlanes [11]      | 31.61               | 0.97            | -                  | 52 mins                    | 0.97           | 418                       |
| HexPlane-Slim [5] | 31.04               | 0.97            | 0.04               | 11m 30s                    | 2.5            | 67                        |
| FFDNeRF [12]      | 32.68               | 0.97            | 0.04               | -                          | < 1            | 440                       |
| MSTH [42]         | 31.34               | 0.98            | 0.02               | 6 mins                     | -              | -                         |
| 3DGS [16]         | 23.19               | 0.93            | 0.08               | 10 mins                    | 170            | 10                        |
| D3DGS [49]        | 39.11               | 0.98            | 0.01               | -                          | 76             | 37                        |
| 4DGS [43]         | 33.03               | 0.98            | 0.02               | 15 mins                    | 78             | 22                        |
| <b>Ours</b>       | 32.56               | 0.96            | 0.03               | 24 mins                    | 89             | 2.21                      |
|                   | 32.77               | 0.97            | 0.03               | 24 mins                    | 87             | 2.69                      |
|                   | 32.99               | 0.98            | 0.02               | 25 mins                    | 84             | 3.66                      |

More hyperparameters will be shown in the Appendix. The implementation of the checkerboard model is based on [4] with a 4x downscaling on the hyperprior, and the *entropy bottleneck* is adopted from [3]. During training, we vary  $\lambda$  from  $5e-5$  to  $5e-2$  and adjust the pruning ratio from 0.19 to 0.64 to achieve different rates.

**Dataset:** For synthetic scene evaluation, we use **D-NeRF** dataset [35], which is designed for monocular view synthesis with 50-200 frames from a single camera. For real-world scenes, we use the **Neu3D** [20] and **HyperNeRF** [32] datasets: Neu3D is captured using 15-20 cameras, while HyperNeRF employs one or two. Data preprocessing and point cloud initialization are conducted as described in [43].

**Baselines:** We compare our method with recent NeRF-based and GS-based dynamic NVS approaches. [1, 10, 12, 22, 31, 32, 35, 41, 42] are SOTA NeRF-based approaches. In the GS-based category, time-variant methods include [21, 27, 40, 46], while [2, 25, 43, 49] are selected as representations of time-invariant methods. Since these approaches lack entropy-constrained optimization, we additionally train the SOTA entropy-constrained 3DGS method, CompGS [24], across multiple frames to serve as a baseline. During evaluation, some methods are tested on specific datasets, as they are designed exclusively for either monocular or multi-camera setups.

**Metrics:** We report the quality of rendered images using

Table 2. Quantitative results on Neu3D dataset, rendering resolution is set to  $1024 \times 768$ .

| Model              | PSNR(dB) $\uparrow$ | D-SSIM $\downarrow$ | LPIPS $\downarrow$ | Training time | FPS $\uparrow$ | Storage (MB) $\downarrow$ |
|--------------------|---------------------|---------------------|--------------------|---------------|----------------|---------------------------|
| DyNeRF [35]        | 29.58               | 0.020               | 0.083              | -             | 0.015          | 28                        |
| NeRFPlayer [39]    | 30.69               | 0.034               | 0.111              | 6 hours       | 0.045          | -                         |
| HyperReel [1]      | 31.10               | 0.036               | 0.096              | 9 hours       | 2.0            | 360                       |
| HexPlane-all [5]   | 31.70               | 0.014               | 0.075              | 12 hours      | 0.2            | 250                       |
| Mixvoxels-X [41]   | 31.73               | -                   | 0.064              | -             | 4.6            | 500                       |
| KPlanes [11]       | 31.63               | -                   | -                  | 1.8 hours     | 0.3            | 309                       |
| Im4D [22]          | 32.58               | 0.020               | 0.208              | ~5 hours      | ~5             | 93                        |
| MSTH [42]          | 32.37               | 0.015               | 0.056              | 20 mins       | 2              | 135                       |
| E-D3DGS [2]        | 31.20               | 0.026               | 0.030              | 2h            | 42             | 40                        |
| STG [21]           | 32.04               | 0.026               | 0.044              | > 8 hours     | 110            | 175                       |
| Dynamic3DGS [27]   | 30.46               | 0.035               | 0.099              | 10 hours      | 460            | 2772                      |
| Real-Time4DGS [46] | 32.01               | 0.014               | 0.055              | 9 hours       | 114            | > 1000                    |
| 3DGSStream [40]    | 31.67               | -                   | -                  | 60 mins       | 215            | 2340                      |
| DN-4DGS [25]       | 32.02               | 0.014               | 0.043              | 50 mins       | 15             | 112                       |
| CompGS [24]        | 29.61               | 0.077               | 0.099              | > 1d          | 45             | ~ 825                     |
| 4DGS [43]          | 31.72               | 0.016               | 0.049              | 40 mins       | 34             | 38                        |
| <b>Ours</b>        | 31.48               | 0.017               | 0.064              | 1.3 hours     | 40             | 3.77                      |
|                    | 31.62               | 0.017               | 0.057              | 1.3 hours     | 39             | 4.38                      |
|                    | 31.69               | 0.016               | 0.053              | 1.3 hours     | 37             | 5.46                      |

Note: Coffee martini is excluded in our evaluation. CompGS is trained every 30 frames for estimation.

peak-signal-to-noise ratio (PSNR), (multiscale) structural similarity index (SSIM), structural dissimilarity index (D-SSIM), perceptual quality measure LPIPS, rendering fps, training time and storage. Three rate-distortion points are displayed for each dataset due to space limitation; detailed rate-distortion results can be found in the Appendix.

**Bitstream:** Light4GS consists of five bitstreams: deformable primitives (excluding SH), a deformation MLP, entropy-coded bitstreams for multiscale hexplanes and SH, and the MHCM. The MHCM, which occupies at most 0.77 MB in our setup, uses separate CNNs for hyperprior and different contexts extraction and distribution prediction. To preserve rendering accuracy, both the MHCM and the primitive’s attributes are stored in float32, except that SH is encoded based on predicted probabilities. AC is applied to encode both multiscale hexplanes and the SH.

## 5.2. Results

According to the quantitative results in Tables 1-3, we observe consistent findings across all datasets that: 1) All NeRF-based methods render at extremely low speeds (< 2fps) due to their cumbersome volumetric rendering pro-

Table 3. Quantitative results on HyperNeRF’s dataset. Rendering resolution is set to 960×540.

| Model           | PSNR(dB)↑ | MS-SSIM↑ | Time↓     | FPS↑ | Storage (MB)↓ |
|-----------------|-----------|----------|-----------|------|---------------|
| Nerfies [31]    | 22.20     | 0.803    | ~ hours   | < 1  | -             |
| HyperNeRF [32]  | 22.40     | 0.814    | 32 hours  | < 1  | -             |
| TiNeuVox-B [10] | 24.30     | 0.836    | 30 mins   | 1    | 48            |
| FFDNeRF [12]    | 24.20     | 0.842    | -         | 0.05 | 440           |
| 3DGS [16]       | 19.70     | 0.680    | 40 mins   | 55   | 52            |
| D3DGS [12]      | 22.40     | 0.612    | -         | 22   | 129           |
| E-D3DGS [2]     | 25.72     | -        | 2 hours   | 26   | 47            |
| DN-4DGS [25]    | 25.59     | 0.861    | 1.2 hours | 20   | 68            |
| 4DGS [43]       | 25.58     | 0.848    | 30 mins   | 22   | 63            |
| Ours            | 25.35     | 0.845    | 50 mins   | 28   | 5.15          |
|                 | 25.46     | 0.845    | 50 mins   | 27   | 6.84          |
|                 | 25.55     | 0.847    | 50 mins   | 27   | 8.87          |

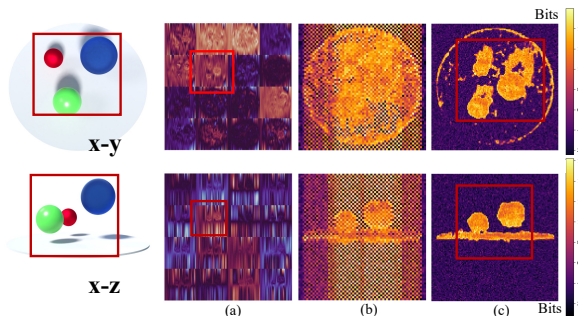


Figure 5. Bitrate allocation visualization (space-only). (a): hex-plane maps; (b) (c): hexplane bitrate maps of low- and high-scales.

cess. NeRFs using low-rank grid representations [5, 11] perform well in synthetic scenes but struggle with convergence in real-world scenes and require 100–132× more storage than our approach. 2) GS-based methods generally offer improved rendering quality and speed compared to NeRFs; however, time-variant methods [27, 40, 46] come with significantly larger model sizes and still encounter convergence issues. For example, [27] demands 735× more storage than our approach, and training [21, 27, 46] requires over 8 hours. Deformation-based methods [2, 25, 43] demonstrate better convergence with slightly lower quality, but they still require up to 10× more storage than our approach. 3) Our method outperforms the entropy-constrained GS method, CompGS [24], on Neu3D with a 6.3% PSNR increase and a 218× storage reduction. This underscores the importance of effective temporal modeling, as CompGS’s intra-entropy constraint restricts its performance compared to most baselines. To summarize, Light4GS achieves substantial compression gains not only over NeRF-based and time-variant GS methods but also provides over 10× compression compared to deformable GSs and 200×+ over entropy-constrained GS, without sacrificing other performance metrics.

**Bitrate Allocation:** We illustrate how MHCM distributes bits across hexplanes in Fig 5. The visualization shows that applying the checkerboard model to the lowest-scale hexplane creates an alternating pattern, where anchor positions

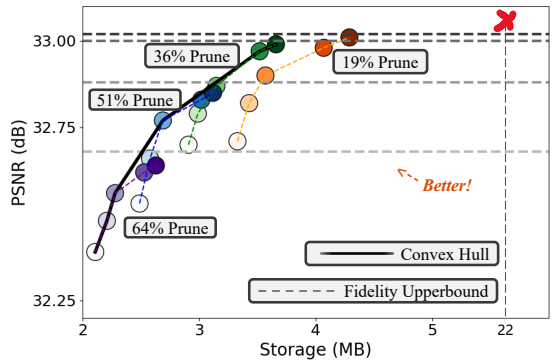


Figure 6. RD-curves and fidelity upperbounds on D-NeRF. STP ratios are denoted by: Orange as 19%, green as 36%, blue as 51% and purple as 64%. Grey dashed lines represent fidelity upperbounds and Red cross denotes no STP and rate-distortion.

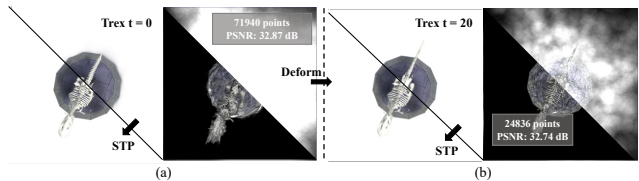


Figure 7. Effects of STP, the first (a) and last deformed frame (b) is displayed as toy examples.

efficiently leverage contextual information for optimized bit allocation compared to non-anchor positions. Additionally, the higher-scale hexplane exhibits substantial bitrate reduction, demonstrating that inter-scale context effectively captures cross-scale similarities. As the impact of inter-plane context is minimal and not easily observed, we defer its discussion to the Ablation Study. These observations affirm the effectiveness and rationale behind our MHCM design.

**Rate-Distortion and Fidelity Upperbound:** To capture the combined rate-distortion of STP, MHCM and entropy-constrained SH compression, we train Light4GS models across various pruning ratios with  $\lambda$  setups. The final optimal rate-distortion curve is constructed by taking the *convex hull* of all resulting points, as illustrated by the solid black line in Fig. 6. Fidelity upperbounds, serving as ground truth for rate-distortion performance, are established by training Light4GS at corresponding pruning ratios with  $\lambda$  equal to 0.

### 5.3. Ablation Study

We conduct detailed introspections of Light4GS’s components and rate-distortion primarily on the D-NeRF dataset for efficiency considerations<sup>1</sup>.

**Impact of STP:** In Fig. 7, we present the first and last deformed frames along with their primitive visualizations under a 64% STP: bottom left is pruned *Trex* vs top right is unpruned *Trex*. Results demonstrate that most primitives have minimal impact on the final rendering. By removing these

<sup>1</sup>If not specified, all ablations are conducted with a 51% STP ratio.

Table 4. Ablation study of **MHCM**. "Entropy" denotes entropy-constrained training.

| Entropy | Checkerboard | Inter-Scale | Inter-Plane | PSNR $\uparrow$ /Size $\downarrow$ |
|---------|--------------|-------------|-------------|------------------------------------|
| ✓       | ✓            | ✓           | ✓           | 0% / 0%                            |
| ✓       | ✓            | ✓           | ✗           | -0.063% / +2.25%                   |
| ✓       | ✓            | ✗           | ✗           | -0.080% / +8.17%                   |
| ✓       | ✗            | ✗           | ✗           | -0.222% / +12.1%                   |
| ✗       | ✗            | ✗           | ✗           | +0.418% / +68.8%                   |

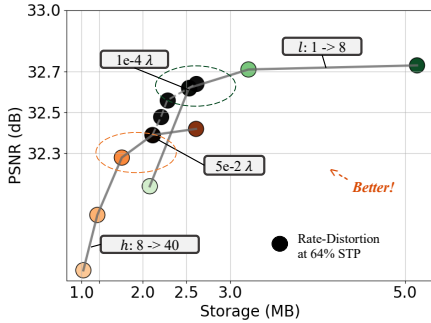


Figure 8. Impact of feature dimension size and multiscale.

insignificant primitives, STP produces a more compact representation, i.e., primitives are distributed to form a defined physical shape with respect to spatial content, with only a slight decrease in rendering quality (-0.07 dB). STP also can improve training efficiency, as fewer primitives need optimization and querying to train multiscale hexplanes.

**Ablation of MHCM:** As shown in Table 4, integrating all deep contexts of MHCM, i.e., checkerboard, inter-scale, and inter-plane, increases the rate-distortion performance. Inter-plane context has the minimal effect, as it applies only to space-only planes at the lowest-scale. The inter-scale context, however, achieves the largest storage savings by eliminating the storage need for high-scale hyperpriors. Although the checkerboard context provides limited storage savings, because the hexplane rate reduction does not offset the increased network size required for context modeling, it has the greatest impact on quality, yielding a 0.14% PSNR increase.

**Ablation of Rate-distortion:** Table 5 demonstrates the effects of various rate-distortion configurations. Results indicate that applying STP alone achieves a 19.2% reduction in storage with a PSNR drop of 0.43%. Adding the rate-distortion constraint for SH increases storage savings to 35.2%, with PSNR drop of 0.60%. The rate-distortion constraint on multiscale hexplane provides even greater storage reductions than those for SH, as SH coefficients are encoded without applying any deep context. Our approach achieves an 83% storage reduction for primitives and a 98% reduction for multiscale hexplane, while resulting in a loss of PSNR at only 8.47%. These findings emphasize how Light4GS effectively balances significant storage savings with high fidelity through the strategic integration of STP and MHCM.

Table 5. Ablation results showing RD-rates, "GS" denotes Gaussian primitives, "Hex" denotes multiscale hexplanes.

| Ablation items             | PSNR $\uparrow$ /Storage $\downarrow$ | GS Size $\downarrow$ | Hex Size $\downarrow$ |
|----------------------------|---------------------------------------|----------------------|-----------------------|
| w/o STP & RD               | 0%/0%                                 | 0%                   | 0%                    |
| STP w/o RD                 | -0.43%/-19.2%                         | -43.9%               | 0%                    |
| STP w/ SH-RD, $c_i$        | -0.60%/-35.2%                         | <b>-81.2%</b>        | 0%                    |
| STP w/ Hex-RD, $R_i$       | -0.66%/-75.4%                         | 56.1%                | <b>-98.7%</b>         |
| STP w/ Full-RD, $R_i, c_i$ | -0.85%/-88%                           | <b>-83.1%</b>        | <b>-98.7%</b>         |

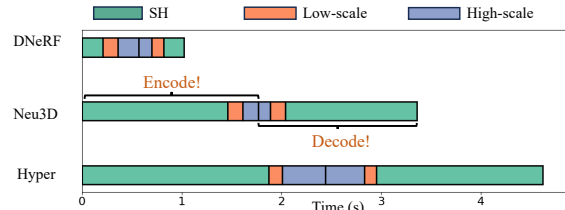


Figure 9. End-to-end coding latency for all scenes. Orange and blue denote coding latencies for hexplanes.

**Impact of Hexplane Features:** To explore the impact of scales  $l$  and the hexplane feature size  $h$ , we train Light4GS models with different values of  $h$  and  $l$ . The black anchors in Fig. 8 represent the trained rate-distortion curve based on our experimental setting of  $h = 32$  and  $l = 2$ . For clearer insights, we conduct ablations for the two parameters at different  $\lambda$ s. Results suggest that our configuration is near the Pareto-optimal region, where increasing the number of scales yields diminishing PSNR gains since higher-scales struggle to capture unique details beyond those at lower-scales, while reducing scales rapidly degrades the rendering quality. A similar trend holds for feature size ablation.

#### 5.4. Coding Complexity

We use *torchac* [34] and the Gaussian conditional codec [4] to encode the SH coefficients of primitives and multiscale hexplanes. As shown in Fig. 9, all scene coding latencies (for either encoding and decoding) remain under 8 ms per frame, enabling real-time streaming for Light4GS. Notably, SH coding operates independently from multiscale hexplane coding, and individual planes of higher-scales can also be coded separately. This independence allows for efficient pipelining of Light4GS coding in practice.

## 6. Conclusion

We propose Light4GS to address the storage and computational demands in dynamic 3DGS, achieving a balanced trade-off between storage efficiency, rendering quality, and computational performance through STP and MHCM. Experiments demonstrate that our approach surpasses existing dynamic NVS methods by delivering higher compression rates with comparable rendering quality. Additionally, entropy-constrained SH compression and adaptive quantization further improve Light4GS's storage efficiency. Since

all deformation-based GS models rely on Gaussian primitives and latent embeddings, our method is expected to serve as a benchmark for compressing this type of models in the future.

## References

- [1] Benjamin Attal, Jia-Bin Huang, Christian Richardt, Michael Zollhoefer, Johannes Kopf, Matthew O’Toole, and Changil Kim. Hyperreel: High-fidelity 6-dof video with ray-conditioned sampling. In *Proceedings of the IEEE/CVF Conference on Computer Vision and Pattern Recognition*, pages 16610–16620, 2023. 6
- [2] Jeongmin Bae, Seoha Kim, Youngsik Yun, Hahyun Lee, Gun Bang, and Youngjung Uh. Per-gaussian embedding-based deformation for deformable 3d gaussian splatting. *arXiv preprint arXiv:2404.03613*, 2024. 2, 6, 7, 11
- [3] Johannes Ballé, David Minnen, Saurabh Singh, Sung Jin Hwang, and Nick Johnston. Variational image compression with a scale hyperprior. *arXiv*, 2018. 5, 6, 11
- [4] Jean Bégaint, Fabien Racapé, Simon Feltman, and Akshay Pushparaja. Compressai: a pytorch library and evaluation platform for end-to-end compression research. *arXiv*, 2020. 6, 8, 11
- [5] Ang Cao and Justin Johnson. Hexplane: A fast representation for dynamic scenes. In *Proceedings of the IEEE/CVF Conference on Computer Vision and Pattern Recognition*, pages 130–141, 2023. 2, 3, 5, 6, 7, 11
- [6] Anpei Chen, Zexiang Xu, Andreas Geiger, Jingyi Yu, and Hao Su. Tensorf: Tensorial radiance fields. In *European conference on computer vision*, pages 333–350. Springer, 2022. 3
- [7] Yihang Chen, Qianyi Wu, Mehrtaash Harandi, and Jianfei Cai. How far can we compress instant-ngp-based nerf? In *Proceedings of the IEEE/CVF Conference on Computer Vision and Pattern Recognition*, pages 20321–20330, 2024. 3
- [8] Yihang Chen, Qianyi Wu, Weiyao Lin, Mehrtaash Harandi, and Jianfei Cai. Hac: Hash-grid assisted context for 3d gaussian splatting compression. In *European Conference on Computer Vision*, pages 422–438. Springer, 2025. 2, 3
- [9] Zhiwen Fan, Kevin Wang, Kairun Wen, Zehao Zhu, De-jia Xu, and Zhangyang Wang. Lightgaussian: Unbounded 3d gaussian compression with 15x reduction and 200+ fps. *arXiv preprint arXiv:2311.17245*, 2023. 2, 11
- [10] Jiemin Fang, Taoran Yi, Xinggang Wang, Lingxi Xie, Xiaoopeng Zhang, Wenyu Liu, Matthias Nießner, and Qi Tian. Fast dynamic radiance fields with time-aware neural voxels. In *SIGGRAPH Asia 2022 Conference Papers*, 2022. 6, 7, 11
- [11] Sara Fridovich-Keil, Giacomo Meanti, Frederik Rahbæk Warburg, Benjamin Recht, and Angjoo Kanazawa. K-planes: Explicit radiance fields in space, time, and appearance. In *Proceedings of the IEEE/CVF Conference on Computer Vision and Pattern Recognition*, pages 12479–12488, 2023. 2, 3, 6, 7
- [12] X. Guo, J. Sun, Y. Dai, G. Chen, X. Ye, X. Tan, E. Ding, Y. Zhang, and J. Wang. Forward flow for novel view synthesis of dynamic scenes. In *Proceedings of the IEEE/CVF International Conference on Computer Vision*, pages 16022–16033, 2023. 6, 7, 11
- [13] Dailan He, Yaoyan Zheng, Baocheng Sun, Yan Wang, and Hongwei Qin. Checkerboard context model for efficient learned image compression. In *Proceedings of the IEEE/CVF Conference on Computer Vision and Pattern Recognition*, pages 14766–14775, 2021. 3, 11
- [14] Dailan He, Ziming Yang, Weikun Peng, Rui Ma, Hongwei Qin, and Yan Wang. Elic: Efficient learned image compression with unevenly grouped space-channel contextual adaptive coding. In *Proceedings of the IEEE/CVF Conference on Computer Vision and Pattern Recognition*, pages 5718–5727, 2022. 3
- [15] He Huang, Wenjie Huang, Qi Yang, Yiling Xu, and Zhu li. A hierarchical compression technique for 3d gaussian splatting compression. *arXiv preprint arXiv:2411.06976*, 2024. 2
- [16] Bernhard Kerbl, Georgios Kopanas, Thomas Leimkühler, and George Drettakis. 3d gaussian splatting for real-time radiance field rendering. *ACM Trans. Graph.*, 42(4):139–1, 2023. 1, 6, 7, 11
- [17] G. G. Langdon. An introduction to arithmetic coding. *IBM Journal of Research and Development*, 28(2):135–149, 1984. 4
- [18] Joo Chan Lee, Daniel Rho, Xiangyu Sun, Jong Hwan Ko, and Eunbyung Park. Compact 3d gaussian representation for radiance field. In *Proceedings of the IEEE/CVF Conference on Computer Vision and Pattern Recognition*, pages 21719–21728, 2024. 2
- [19] Jiahao Li, Bin Li, and Yan Lu. Deep contextual video compression. *Advances in Neural Information Processing Systems*, 34, 2021. 3
- [20] Tianye Li, Mira Slavcheva, Michael Zollhoefer, Simon Green, Christoph Lassner, Changil Kim, Tanner Schmidt, Steven Lovegrove, Michael Goesele, Richard Newcombe, et al. Neural 3d video synthesis from multi-view video. In *Proceedings of the IEEE/CVF Conference on Computer Vision and Pattern Recognition*, pages 5521–5531, 2022. 6, 11
- [21] Zhan Li, Zhang Chen, Zhong Li, and Yi Xu. Spacetime gaussian feature splatting for real-time dynamic view synthesis. In *Proceedings of the IEEE/CVF Conference on Computer Vision and Pattern Recognition*, pages 8508–8520, 2024. 2, 6, 7, 11
- [22] Haotong Lin, Sida Peng, Zhen Xu, Tao Xie, Xingyi He, Hujun Bao, and Xiaowei Zhou. High-fidelity and real-time novel view synthesis for dynamic scenes. In *SIGGRAPH Asia Conference Proceedings*, 2023. 6
- [23] Mufan Liu, Le Yang, Yiling Xu, Ye-kui Wang, and Jenq-Neng Hwang. Evan: Evolutional video streaming adaptation via neural representation. *arXiv preprint arXiv:2406.02557*, 2024. 2
- [24] Xiangrui Liu, Xinju Wu, Pingping Zhang, Shiqi Wang, Zhu Li, and Sam Kwong. Compgs: Efficient 3d scene representation via compressed gaussian splatting. In *Proceedings of the 32nd ACM International Conference on Multimedia*, 2024. 2, 6, 7, 11

- [25] Jiahao Lu, Jiacheng Deng, Ruijie Zhu, Yanzhe Liang, Wenfei Yang, Tianzhu Zhang, and Xu Zhou. Dn-4dgs: Denoised deformable network with temporal-spatial aggregation for dynamic scene rendering. *arXiv preprint arXiv:2410.13607*, 2024. 6, 7
- [26] Tao Lu, Mulin Yu, Linning Xu, Yuanbo Xiangli, Limin Wang, Dahua Lin, and Bo Dai. Scaffold-gs: Structured 3d gaussians for view-adaptive rendering. In *Proceedings of the IEEE/CVF Conference on Computer Vision and Pattern Recognition*, pages 20654–20664, 2024. 2
- [27] Jonathon Luiten, Georgios Kopanas, Bastian Leibe, and Deva Ramanan. Dynamic 3d gaussians: Tracking by persistent dynamic view synthesis. In *2024 International Conference on 3D Vision (3DV)*, pages 800–809. IEEE, 2024. 6, 7
- [28] Ben Mildenhall, Pratul P Srinivasan, Matthew Tancik, Jonathan T Barron, Ravi Ramamoorthi, and Ren Ng. Nerf: Representing scenes as neural radiance fields for view synthesis. *Communications of the ACM*, 65(1):99–106, 2021. 1
- [29] Thomas Müller, Alex Evans, Christoph Schied, and Alexander Keller. Instant neural graphics primitives with a multiresolution hash encoding. *ACM transactions on graphics (TOG)*, 41(4):1–15, 2022. 2
- [30] Simon Niedermayr, Josef Stumpfegger, and Rüdiger Westermann. Compressed 3d gaussian splatting for accelerated novel view synthesis. *arXiv preprint arXiv:2401.02436*, 2023. 2
- [31] Keunhong Park, Utkarsh Sinha, Jonathan T Barron, Sofien Bouaziz, Dan B Goldman, Steven M Seitz, and Ricardo Martin-Brualla. Nerfies: Deformable neural radiance fields. In *Proceedings of the IEEE/CVF International Conference on Computer Vision*, pages 5865–5874, 2021. 6, 7
- [32] Keunhong Park, Utkarsh Sinha, Peter Hedman, Jonathan T Barron, Sofien Bouaziz, Dan B Goldman, Ricardo Martin-Brualla, and Steven M Seitz. Hypernerf: A higher-dimensional representation for topologically varying neural radiance fields. *arXiv preprint arXiv:2106.13228*, 2021. 6, 7, 11
- [33] Grzegorz Pastuszak and Andrzej Abramowski. Algorithm and architecture design of the h.265/hevc intra encoder. *IEEE Transactions on Circuits and Systems for Video Technology*, 26(1):210–222, 2016. 2
- [34] Adam Paszke, Sam Gross, Soumith Chintala, Gregory Chanan, Edward Yang, Zachary DeVito, Zeming Lin, Alban Desmaison, Luca Antiga, and Adam Lerer. Automatic differentiation in pytorch. In *NIPS-W*, 2017. 5, 8
- [35] Albert Pumarola, Enric Corona, Gerard Pons-Moll, and Francesc Moreno-Noguer. D-nerf: Neural radiance fields for dynamic scenes. *arXiv preprint arXiv:2011.13961*, 2020. 6, 11
- [36] Kerui Ren, Lihan Jiang, Tao Lu, Mulin Yu, Linning Xu, Zhangkai Ni, and Bo Dai. Octree-gs: Towards consistent real-time rendering with lod-structured 3d gaussians. *arXiv*, 2024. 2
- [37] Daniel Rho, Byeonghyeon Lee, Seungtae Nam, Joo Chan Lee, Jong Hwan Ko, and Eunbyung Park. Masked wavelet representation for compact neural radiance fields. In *Proceedings of the IEEE/CVF Conference on Computer Vision and Pattern Recognition*, pages 20680–20690, 2023. 3
- [38] Seungjoo Shin and Jaesik Park. Binary radiance fields. *Advances in neural information processing systems*, 36, 2024. 2
- [39] Liangchen Song, Anpei Chen, Zhong Li, Zhang Chen, Lele Chen, Junsong Yuan, Yi Xu, and Andreas Geiger. Nerf-player: A streamable dynamic scene representation with decomposed neural radiance fields. *IEEE Transactions on Visualization and Computer Graphics*, 29(5):2732–2742, 2023. 1, 6
- [40] Jiakai Sun, Han Jiao, Guangyuan Li, Zhanjie Zhang, Lei Zhao, and Wei Xing. 3dstream: On-the-fly training of 3d gaussians for efficient streaming of photo-realistic free-viewpoint videos. In *Proceedings of the IEEE/CVF Conference on Computer Vision and Pattern Recognition*, pages 20675–20685, 2024. 6, 7
- [41] Feng Wang, Sinan Tan, Xinghang Li, Zeyue Tian, and Huaping Liu. Mixed neural voxels for fast multi-view video synthesis. *arXiv preprint arXiv:2212.00190*, 2022. 6, 11
- [42] Feng Wang, Zilong Chen, Guokang Wang, Yafei Song, and Huaping Liu. Masked space-time hash encoding for efficient dynamic scene reconstruction. *Advances in Neural Information Processing Systems*, 36, 2024. 6
- [43] Guanjun Wu, Taoran Yi, Jiemin Fang, Lingxi Xie, Xiaopeng Zhang, Wei Wei, Wenyu Liu, Qi Tian, and Xinggang Wang. 4d gaussian splatting for real-time dynamic scene rendering. In *Proceedings of the IEEE/CVF Conference on Computer Vision and Pattern Recognition*, pages 20310–20320, 2024. 2, 5, 6, 7
- [44] Shuzhao Xie, Weixiang Zhang, Chen Tang, Yunpeng Bai, Rongwei Lu, Shijia Ge, and Zhi Wang. Mesongs: Post-training compression of 3d gaussians via efficient attribute transformation. In *European Conference on Computer Vision*, pages 434–452. Springer, 2025. 2
- [45] Jiawei Xu, Zexin Fan, Jian Yang, and Jin Xie. Grid4d: 4d decomposed hash encoding for high-fidelity dynamic gaussian splatting. *arXiv*, 2024. 2
- [46] Jinbo Yan, Rui Peng, Luyang Tang, and Ronggang Wang. 4d gaussian splatting with scale-aware residual field and adaptive optimization for real-time rendering of temporally complex dynamic scenes. In *Proceedings of the 32nd ACM International Conference on Multimedia*, pages 7871–7880, 2024. 6, 7
- [47] Qi Yang, Kaifa Yang, Yuke Xing, Yiling Xu, and Zhu Li. A benchmark for gaussian splatting compression and quality assessment study. *arXiv*, 2024. 2
- [48] Zeyu Yang, Hongye Yang, Zijie Pan, and Li Zhang. Real-time photorealistic dynamic scene representation and rendering with 4d gaussian splatting. *arXiv preprint arXiv:2310.10642*, 2023. 2
- [49] Ziyi Yang, Xinyu Gao, Wen Zhou, Shaohui Jiao, Yuqing Zhang, and Xiaogang Jin. Deformable 3d gaussians for high-fidelity monocular dynamic scene reconstruction. In *Proceedings of the IEEE/CVF Conference on Computer Vision and Pattern Recognition*, pages 20331–20341, 2024. 2, 6

## Appendix

This is the supplementary material for Light4GS. Herein, we offer more details about Light4GS implementation, training and evaluation.

### A.1. Training Process

**D-NeRF [35]:** During the first 3000 iterations, only the standard training process of vanilla 3DGS is applied without any additional techniques. From iterations 3000 to 30000, Spatio-Temporal significance Pruning (STP) is performed twice based on a predefined ratio, and primitives are densified every 3000 iterations until 14000 iterations. The entropy constraints of the Multiscale Hexplane Context Model (MHCM) and SH are applied every 3 iterations, with the SH constraint activated only after densification ends. Adaptive quantization starts at 15000 iterations, with the SH quantization fixed at 0.02 based on pre-evaluation of primitives generated from vanilla 4DGS.

**Neu3D and HyperNeRF [20, 32]:** The training pipeline for the two real-world datasets follows that of D-NeRF, with the only modification being a reduction in training iterations to 20,000.

### A.2. Rate-Distortion

The total rate-distortion of Light4GS is determined by three key components: SH coefficients, multiscale hexplanes, and STP. The distortion introduced by STP is controlled by predefined pruning ratios, while the distortion from SH coefficients and multiscale hexplanes is influenced by the parameters  $\lambda$ . In the experiments, the pruning ratios are set to [0.19, 0.36, 0.51, 0.64], with  $\lambda$  selected from [5e-2, 1e-2, 5e-3, 1e-3, 5e-4]. The final rate-distortion curve is constructed by taking the convex hull of all trained rate-distortion points.

As shown in Fig. 10-12, on D-NeRF, Light4GS achieves over a 10 $\times$  reduction in storage compared to 4DGS and HexPlane while preserving competitive visual quality. For Neu3D (Fig. 11), Light4GS demonstrates an 11 $\times$  reduction in model size relative to 4DGS and achieves an impressive 48 $\times$  storage reduction over the time-variant 3DGS STG [21]. For HyperNeRF (Fig. 12), Light4GS achieves a 16 $\times$  storage reduction compared to 4DGS and a 15 $\times$  reduction relative to per-frame training 3DGS [16]. In complex scenes, Light4GS presents notable benefits as the requirement for additional scales to capture details increases inter-scale similarities, thus improving compression efficiency.

### A.3. More Implementation Details

**STP implementation:** We implement STP based on Light-Gaussian [9], where the significance of each primitive is determined by counting the number of intersected pixels.

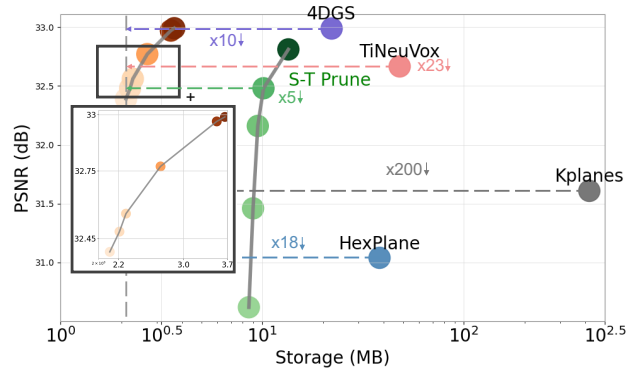


Figure 10. Rate-distortion performance comparison for D-NeRF. Green anchors denote STP only.

This straightforward yet effective criterion has proven to be a practical guideline for primitive pruning. Notably, STP is applied only after the cloning process for primitives has been completed.

**MHCM Implementation:** Our deep context model, MHCM, is built on the *compressai* framework [4]. The hyperprior’s encoding  $h_a()$  and decoding network  $h_s()$ , as well as the entropy model configuration, adhere to the configuration established in [3], employing a hyperprior size that involves 4 $\times$  downsampling. To extract deep context across multiple scales, we employ a simple CNN kernel, where the number of output channels is twice that of the input channels. The checkerboard design uses a multiplexer to accelerate both the encoding and decoding processes [13]. However, when the hexplane dimensions are odd, this can disrupt the multiplexing condition. To mitigate this, we pad the hexplane to ensure it has even dimensions, which, in practice, may slightly increase the encoding bitrate.

### A.4. Qualitative Quality Comparisons

The qualitative results for Light4GS are recorded with setups of  $\lambda = 0.01$  and a pruning ratio of 0.4, where the efficiency of the rate is considered to be prioritized. Quantitative quality comparisons on D-NeRF is presented in Fig. 15, Neu3D in Fig.16-18 and HyperNeRF in Fig. 19.

### A.5. More Visualization Details

Fig. 13 offers an in-depth representation of bitrate allocation for the Trex scene. Fig. 14 provides quantitative quality evaluations on rate-distortion performance, derived from training data on *Flame Steak* and *Cook Spinach*.

### A.6. Per Scene Evaluation

Per scene evaluation [2, 5, 10–12, 24, 41] of Light4GS of all datasets are listed in Table 7-9. Results of “ours” refer to

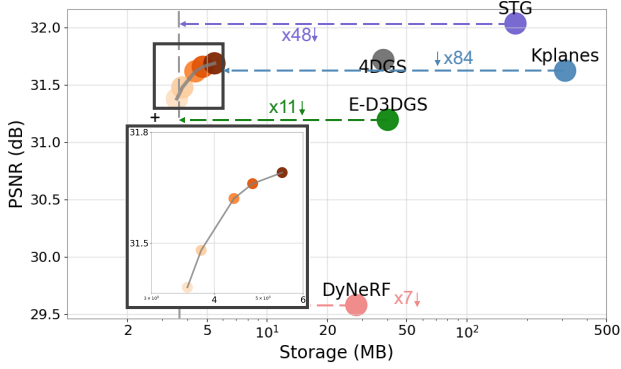


Figure 11. Rate-distortion performance comparison for Neu3D.

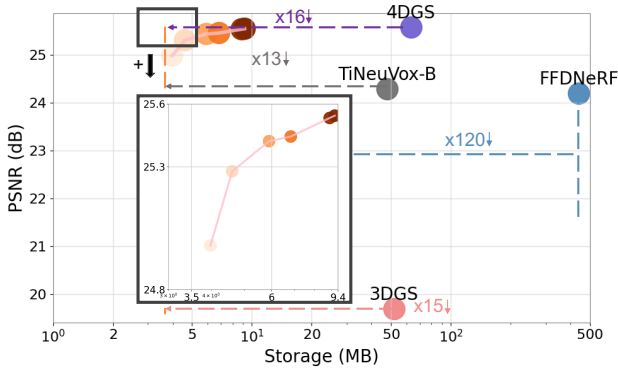


Figure 12. Rate-distortion performance comparison for HyperNeRF.

those that appear in the main text.

### A.7. Bitstream Composition

We present the bitstream composition of all tested scenes in Fig. 20-21. The bitstream is divided into four main components: deformation (deformation network), entropy, hexplane (multiscale hexplanes), and GS (Gaussian primitives). Among these, entropy represents the size of the total multiscale hexplane context model (Entropy model + Conv + MLP). This analysis provides insights into the storage proportions and the relative contributions of each component. Across all scenes, GS consistently accounts for the largest proportion of the bitstream, due to the lack of context modeling in SH compression. The contributions of deformation and hexplane vary slightly across scenes. For scenes with more dynamic content, such as *jumpingjacks*, *mutant*, and *standup*, the proportion of deformation increases, reflecting its critical role in capturing temporal changes caused by object motion or deformation. Meanwhile, *Hexplane* contributes more prominently in scenes requiring detailed spatial adjustments, as observed in *bouncingballs* and *hook*, where finer geometry and motion details are essential for

| No. of points     | 120000 | 80000 | 40000 | 20000 |
|-------------------|--------|-------|-------|-------|
| Deformation (%)   | 1.00   | 1.14  | 1.18  | 1.32  |
| Rasterization (%) | 1.00   | 1.42  | 3.44  | 6.01  |

Table 6. Effect of number of points on rendering FPS.

accurate reconstruction.

### A.8. Bottleneck for rendering speed

We evaluate FPS for both deformation and rasterization, the observations are: 1) deformation is 3-4 times slower than rasterization, and 2) point count affects rasterization FPS linearly, while it has minimal impact on deformation. Thus, we believe that deformation is the main FPS bottleneck, and our pruning method can integrate with faster deformation techniques to show its effectiveness.

### A.9. Limitations

Light4GS serves as a valuable compression benchmark for deformable 3DGS. Although Light4GS achieves comparable rate-distortion performance and effective quality-rate regulation, its flexibility is limited by the separate handling of STP and MHCM. Our Light4GS requires variations for both the rate-distortion trade-off weight and discrete pruning ratios, which complicates the rate-distortion control. Future improvements could involve designing a learnable pruning process that enables jointly rate-distortion control of both pruning and the context modeling. Additionally, due to the randomness of structure-from-motion initialization, the rate-distortion performance cannot be consistently maintained and may vary across different trials. This is an inherent issue in the current GS framework that is expected to be addressed in future works. Moreover, this study does not improve the fidelity upperbound of the original 4DGS, leaving room for further improvements in 4DGS reconstruction quality.

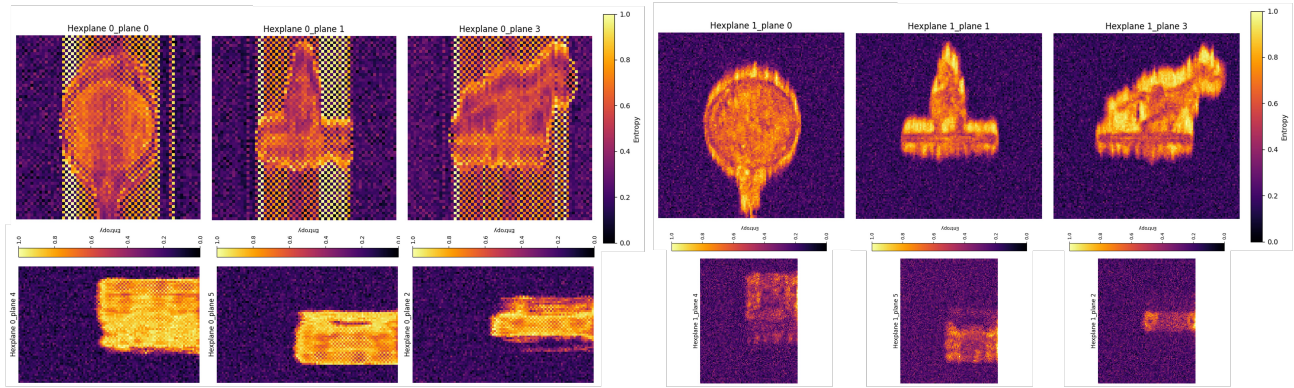


Figure 13. Bitrate allocation for *Trex* trained at two scales (low scale on the left, high scale on the right). Top row: space-only planes; Bottom row: space-time planes. Bitrate map is normalized.

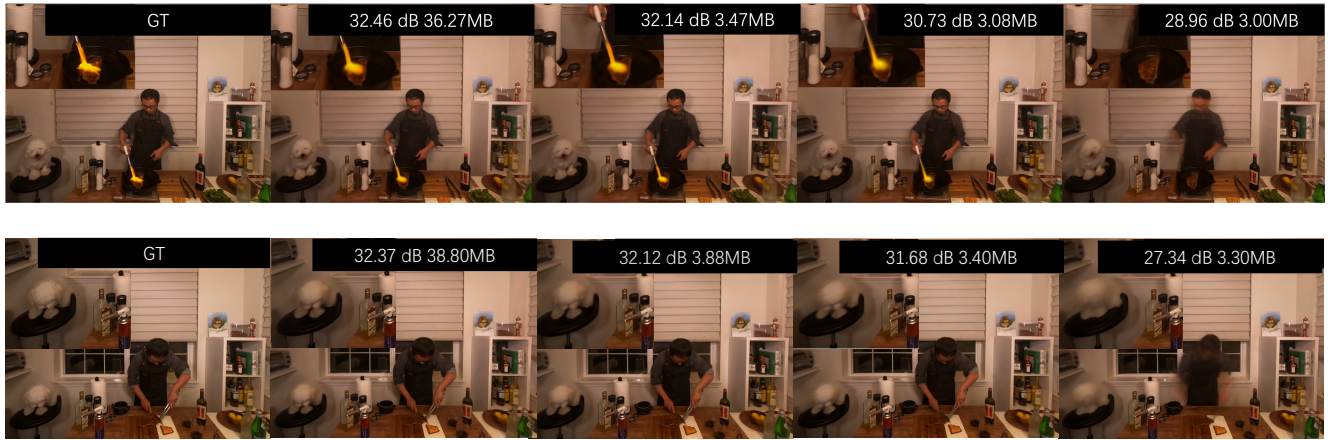


Figure 14. Quantitative quality evaluation of rate-distortion. Top row: *Flame Steak*; Bottom row: *Cook Spinach*.

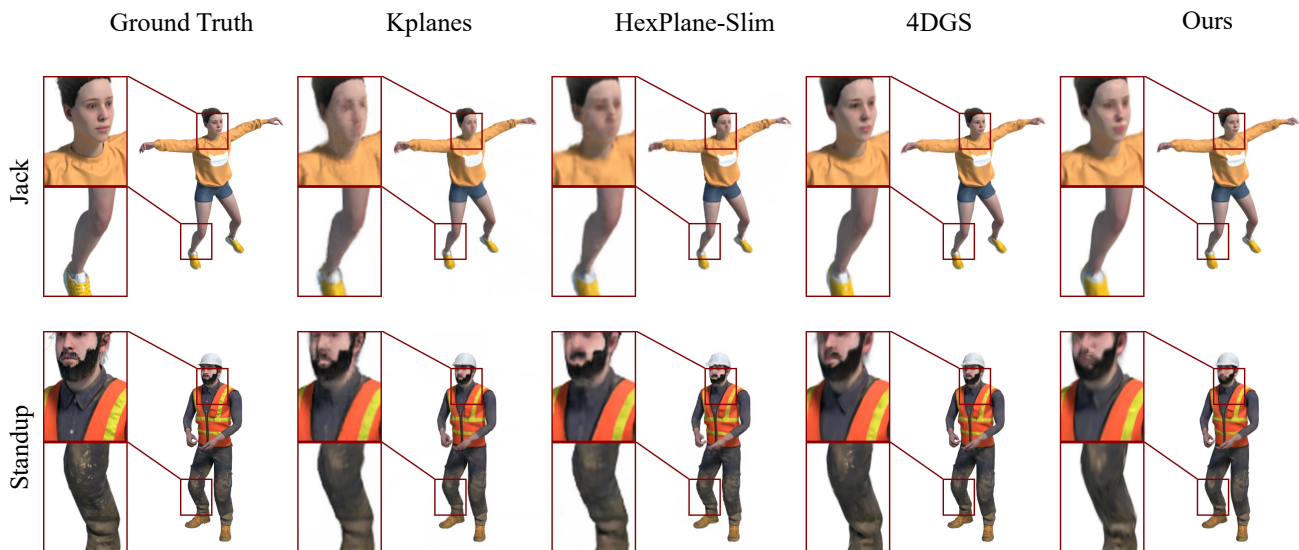


Figure 15. Quantitative quality evaluation of D-NeRF.

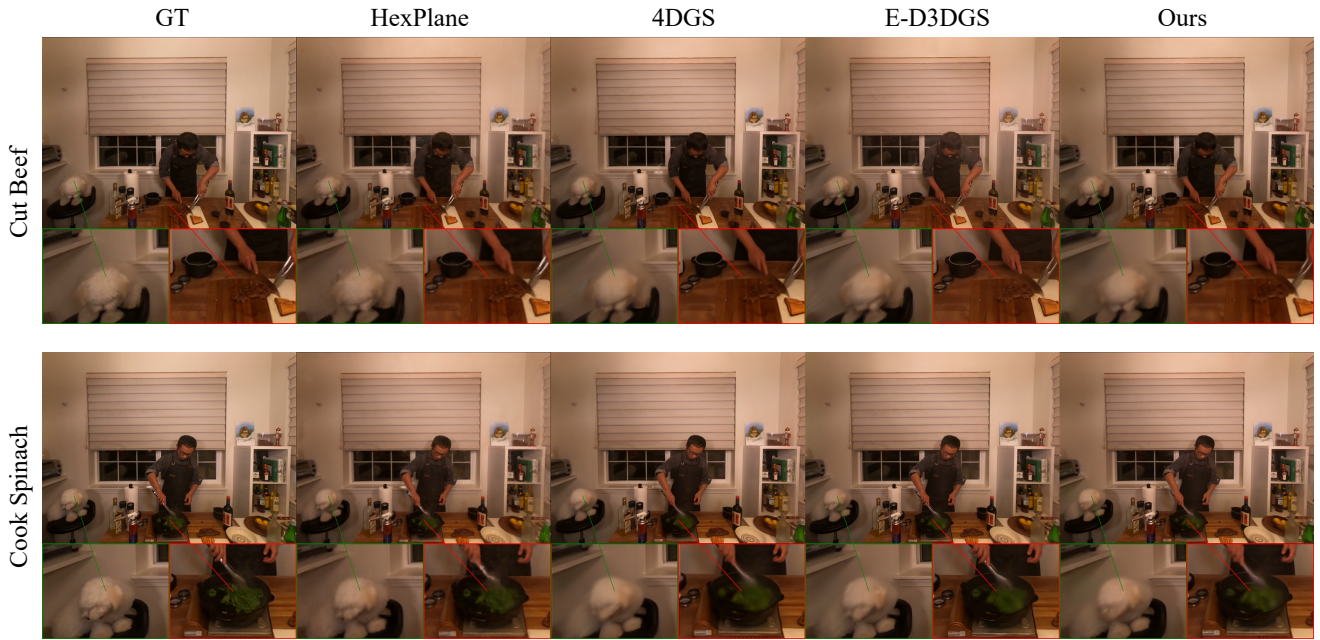


Figure 16. Quantitative quality evaluation of Neu3D.

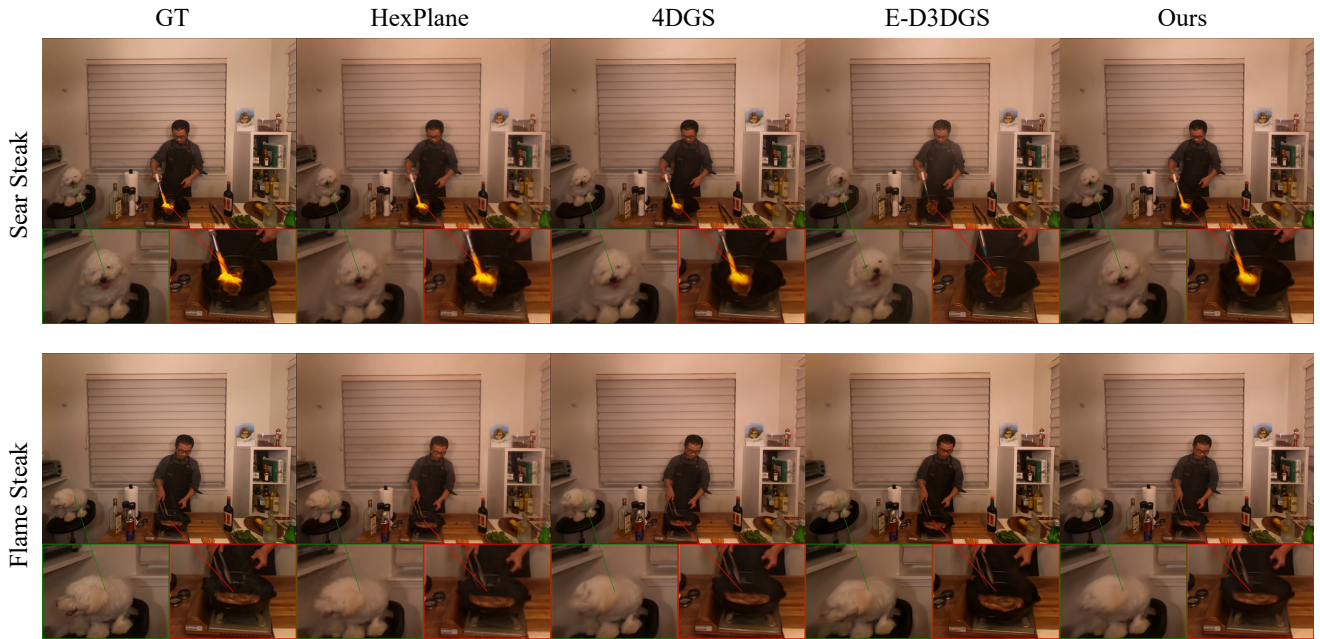


Figure 17. Quantitative quality evaluation of Neu3D.

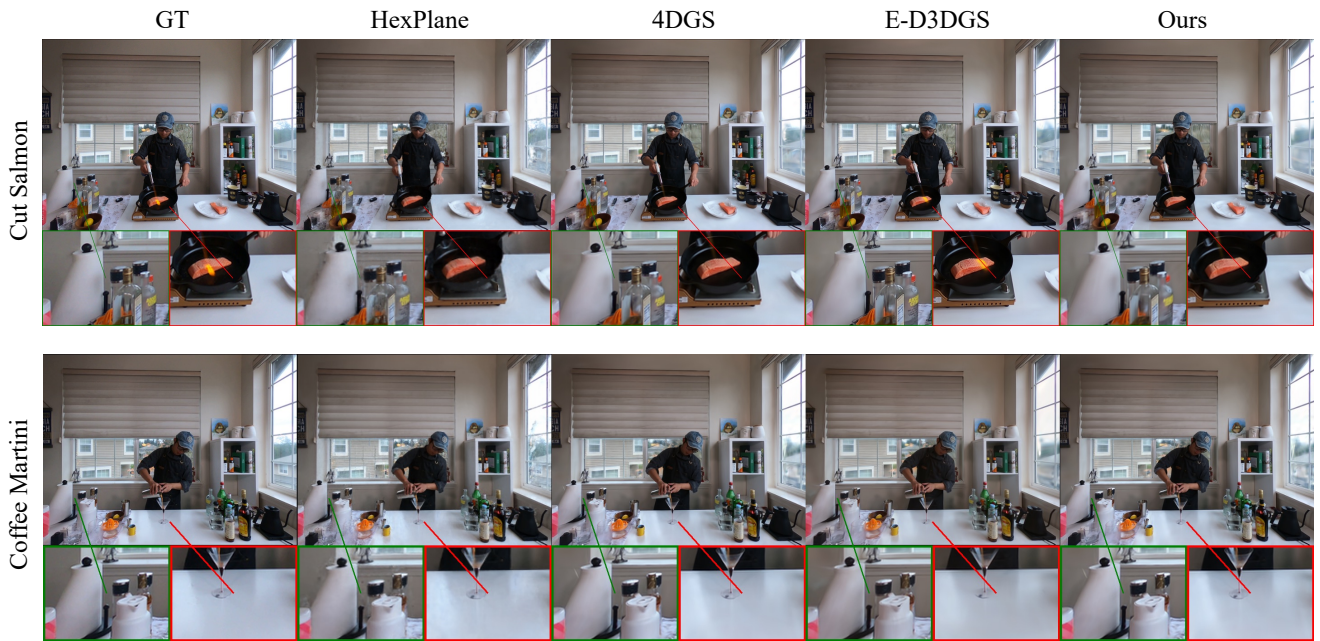


Figure 18. Quantitative quality evaluation of Neu3D.

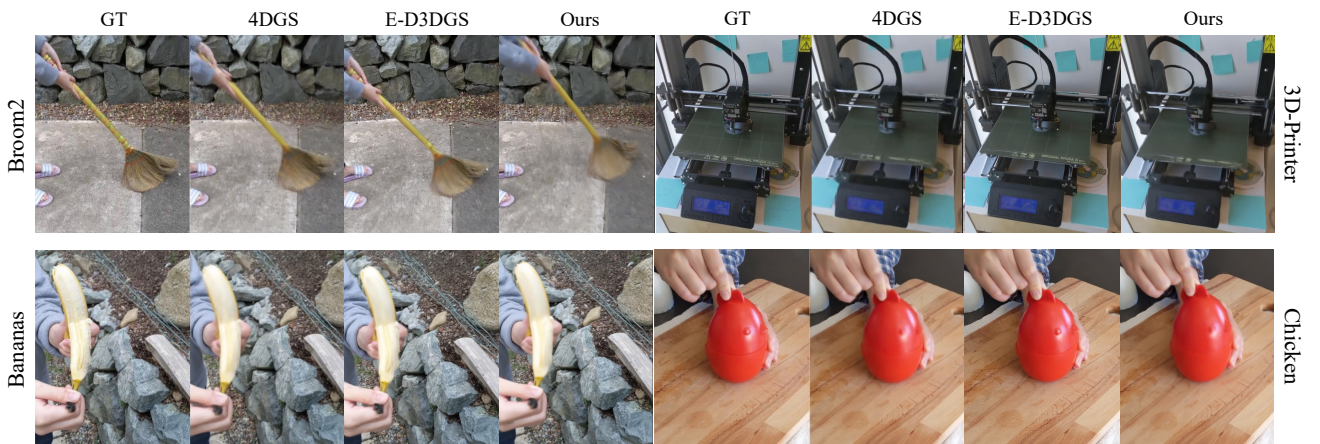


Figure 19. Quantitative quality evaluation of HyperNeRF.

Table 7. Per scene evaluation with PSNR and Storage (MB) on D-NeRF.

| Method          | Bouncing Balls |              | Hellwarrior |              | Hook    |              | Jumpingjacks |              |
|-----------------|----------------|--------------|-------------|--------------|---------|--------------|--------------|--------------|
|                 | PSNR           | Storage (MB) | PSNR        | Storage (MB) | PSNR    | Storage (MB) | PSNR         | Storage (MB) |
| <b>K-Planes</b> | 38.98          | 471.1 MB     | 24.72       | 444.8 MB     | 28.20   | 444.8 MB     | 32.00        | 497.5 MB     |
| <b>HexPlane</b> | 39.86          | 34 MB        | 24.55       | 34 MB        | 28.63   | 34 MB        | 31.31        | 34 MB        |
| <b>TiNeuVox</b> | 40.23          | 48 MB        | 27.10       | 48 MB        | 28.63   | 48 MB        | 33.49        | 48 MB        |
| <b>4DGS</b>     | 40.18          | 18.94 MB     | 28.97       | 20.3 MB      | 32.19   | 19.78 MB     | 34.35        | 20.31 MB     |
| <b>Ours</b>     | 39.57          | 1.90 MB      | 28.50       | 2.18 MB      | 31.34   | 2.04 MB      | 33.86        | 1.71 MB      |
|                 | 39.88          | 2.19 MB      | 28.72       | 2.54 MB      | 31.58   | 2.46 MB      | 34.12        | 1.97 MB      |
|                 | 40.01          | 2.85 MB      | 28.92       | 3.43 MB      | 31.94   | 3.37 MB      | 34.35        | 2.52 MB      |
| Method          | Lego           |              | Mutant      |              | Standup |              | Trex         |              |
|                 | PSNR           | Storage (MB) | PSNR        | Storage (MB) | PSNR    | Storage (MB) | PSNR         | Storage (MB) |
| <b>K-Planes</b> | 25.46          | 418.4 MB     | 33.55       | 471.1 MB     | 33.27   | 471.1 MB     | 31.28        | 497.5 MB     |
| <b>HexPlane</b> | 25.10          | 34 MB        | 33.67       | 34 MB        | 34.40   | 34 MB        | 30.67        | 34 MB        |
| <b>TiNeuVox</b> | 24.65          | 48 MB        | 30.87       | 48 MB        | 34.61   | 48 MB        | 31.25        | 48 MB        |
| <b>4DGS</b>     | 25.19          | 30.38 MB     | 35.10       | 21.31 MB     | 35.56   | 18.94 MB     | 32.71        | 30.41 MB     |
| <b>Ours</b>     | 25.16          | 3.38 MB      | 34.29       | 1.96 MB      | 34.77   | 1.73 MB      | 32.64        | 2.90 MB      |
|                 | 25.36          | 4.50 MB      | 34.56       | 2.30 MB      | 35.04   | 2.25 MB      | 32.89        | 3.52 MB      |
|                 | 25.53          | 6.38 MB      | 34.79       | 3.21 MB      | 35.28   | 2.54 MB      | 33.12        | 4.98 MB      |

Table 8. Per scene evaluation with PSNR and Storage (MB) on Neu3D.

| Method           | Cut Roasted Beef |              | Cook Spinach |              | Sear Steak |              | Flame Steak |              | Flame Salmon |              |
|------------------|------------------|--------------|--------------|--------------|------------|--------------|-------------|--------------|--------------|--------------|
|                  | PSNR             | Storage (MB) | PSNR         | Storage (MB) | PSNR       | Storage (MB) | PSNR        | Storage (MB) | PSNR         | Storage (MB) |
| <b>HexPlane</b>  | 32.71            | 312.17 MB    | 31.86        | 312.17 MB    | 31.92      | 312.17 MB    | 32.09       | 312.17 MB    | 29.26        | 312.17 MB    |
| <b>KPlanes</b>   | 31.82            | 579.7 MB     | 32.60        | 579.7 MB     | 32.52      | 579.7 MB     | 32.39       | 579.7 MB     | 30.44        | 579.7 MB     |
| <b>MixVoxels</b> | 31.30            | 500 MB       | 31.65        | 500 MB       | 31.43      | 500 MB       | 31.21       | 500 MB       | 29.92        | 500 MB       |
| <b>4DGS</b>      | 32.37            | 38.80 MB     | 32.41        | 38.28 MB     | 32.70      | 36.16 MB     | 31.86       | 36.16 MB     | 29.26        | 38.46 MB     |
| <b>CompGS</b>    | 29.90            | 810 MB       | 30.75        | 824 MB       | 31.23      | 822 MB       | 30.96       | 825 MB       | 25.20        | 864 MB       |
| <b>E-D3DGS</b>   | 29.70            | 39.30 MB     | 32.50        | 39.04 MB     | 32.74      | 28.59 MB     | 31.71       | 36.40 MB     | 29.46        | 68.30 MB     |
| <b>Ours</b>      | 31.84            | 3.90 MB      | 32.44        | 3.89 MB      | 32.40      | 3.51 MB      | 31.60       | 3.61 MB      | 29.14        | 3.96 MB      |
|                  | 31.88            | 4.93 MB      | 32.58        | 4.76 MB      | 32.54      | 4.08 MB      | 31.74       | 3.69 MB      | 29.17        | 4.45 MB      |
|                  | 32.05            | 6.39 MB      | 32.65        | 6.18 MB      | 32.61      | 5.33 MB      | 31.83       | 3.85 MB      | 29.33        | 5.54 MB      |

Table 9. Per scene evaluation with PSNR and Storage (MB) on HyperNeRF.

| Method            | 3D Printer |              | Chicken |              | Broom |              | Banana |              |
|-------------------|------------|--------------|---------|--------------|-------|--------------|--------|--------------|
|                   | PSNR       | Storage (MB) | PSNR    | Storage (MB) | PSNR  | Storage (MB) | PSNR   | Storage (MB) |
| <b>TiNeuVox-B</b> | 22.8       | 48 MB        | 28.3    | 48 MB        | 21.5  | 48 MB        | 24.4   | 48 MB        |
| <b>FFDNeRF</b>    | 22.8       | 440 MB       | 28.0    | 440 MB       | 21.9  | 440 MB       | 24.3   | 440 MB       |
| <b>4DGS</b>       | 22.12      | 63.50 MB     | 29.03   | 90.57 MB     | 22.14 | 46.70 MB     | 29.06  | 51.73 MB     |
| <b>E-D3DGS</b>    | 22.97      | 28.5 MB      | 30.05   | 51.0 MB      | 21.70 | 31.60 MB     | 28.98  | 73.20 MB     |
| <b>Ours</b>       | 21.96      | 6.13 MB      | 28.83   | 4.10 MB      | 22.14 | 2.98 MB      | 28.50  | 7.40 MB      |
|                   | 22.02      | 7.84 MB      | 28.93   | 5.87 MB      | 22.14 | 4.63 MB      | 28.79  | 9.05 MB      |
|                   | 22.08      | 9.50 MB      | 28.97   | 6.98 MB      | 22.16 | 6.10 MB      | 28.99  | 12.98 MB     |

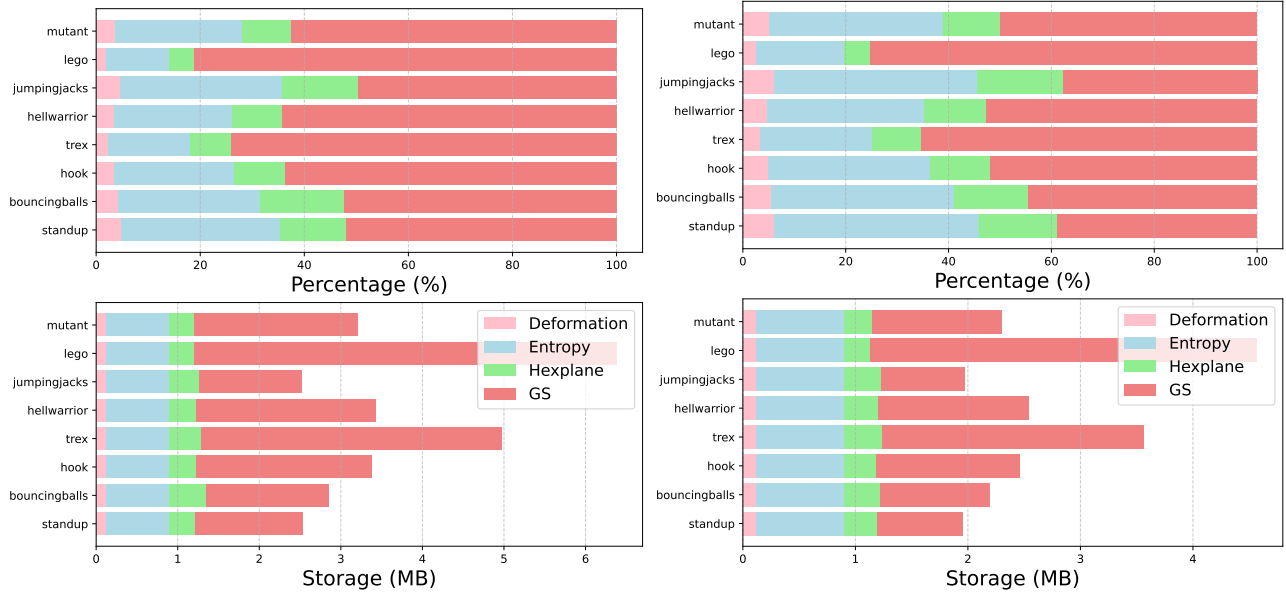


Figure 20. Per scene bitstream composition on D-NeRF (left vs right: two RD points).

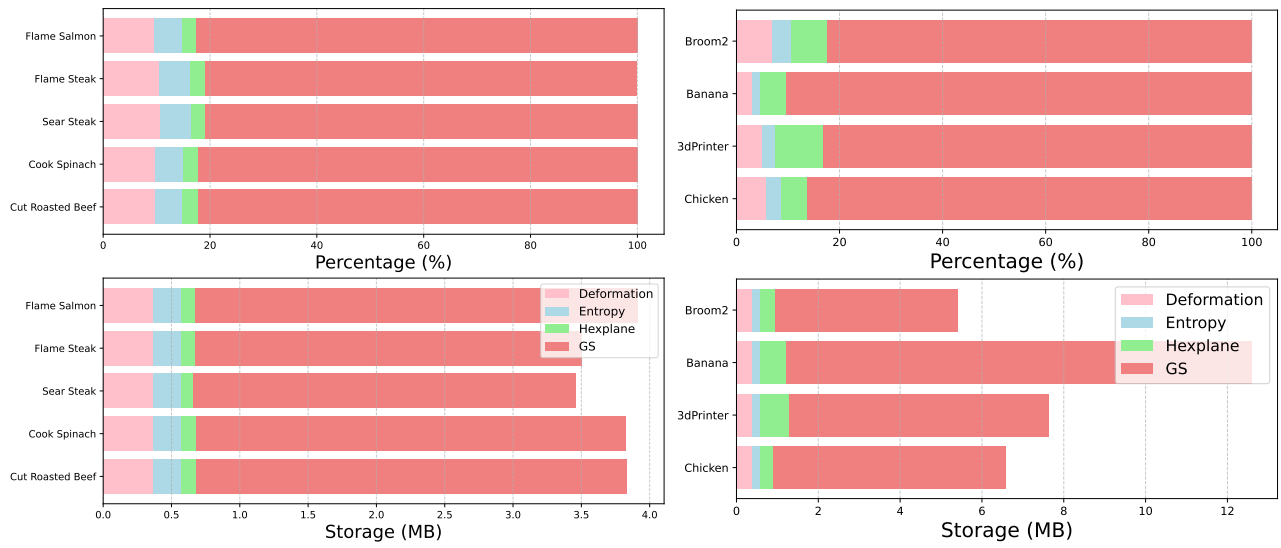


Figure 21. Per scene bitstream composition on Neu3D (left) and HyperNeRF (right).